Silicon (2022) 14:5941–5949
https://doi.org/10.1007/s12633-021-01367-y

ORIGINAL PAPER

60 GHz Double Deck T-Gate AlN/GaN/AlGaN HEMT for V-Band Satellites

A. S. Augustine Fletcher[1] · D. Nirmal[1] · J. Ajayan[2] · L. Arivazhagan[3] · K. Husna Hamza[1] · P. Murugapandiyan[4]

Received: 17 June 2021 / Accepted: 30 August 2021 / Published online: 13 September 2021

Abstract
The influence of double deck T-gate on L_G = 0.2 μm AlN/GaN/AlGaN HEMT is analysed in this paper. The T-gate supported with Silicon Nitride provides a tremendous mechanical reliability. It drops off the crest electric-field at gate edges and postponing the breakdown voltage of a device. A 0.2-μm double deck T-gate HEMT on Silicon Carbide substrate offer f_{MAX} of 107 Giga Hertz, f_T of 60 Giga Hertz and the breakdown voltage of 136 Volts. Furthermore, it produces the maximum-transconductance and drain-current of 0.187 Siemens/mm and 0.41 Ampere/mm respectively. In addition, the lateral electric-field noticed at gate-edge shows 2.1 × 10^6 Volts/cm. Besides, the double deck T-gate AlN/GaN HEMT achieves a 45% increment in breakdown voltage compared to traditional GaN-HEMT device. Moreover, it reveals a remarkable Johnson figure-of-merit of 7.9 Tera Hertz Volt. Therefore, the double deck T-gate on AlN/GaN/AlGaN HEMT is the superlative device for 60 GHz V-band satellite application.

Keywords Cut off frequency · GaN HEMT · T-gate · Electric field · Double deck T-gate · Johnson figure of merit (JFOM) and breakdown voltage

1 Introduction

The constraints of traditional semiconductor devices for Radio frequency and high power microwave application have fashioned the opportunity for wide-bandgap semiconductor materials such as Silicon Carbide, Gallium Nitride (GaN), etc. [1–5]. Gallium Nitride based HEMT devices are attractive for high-frequency and high-power application due to its ultimate material features such as excessive mobility of electron, high breakdown strength, high thermal-conductivity and high saturation velocity of electron [5–10]. Gate geometric engineering is a well known technique to enhance the performance of RF and high power devices. Assorted gating effects are achieved using i) T-gate [11] ii) Pi-gate [12] iii) gamma gate [13] iv) camel gate [14] v) gate field plate [15] vi) discrete field plate [16] vii) and multiple grating field plate [17]. The extension of gate head serves as a gate field plate. It suppresses the dispersion and electric field to improve the device reliability [18]. Pi-gate restricts the electron acceleration near the gate edges reducing the hot electron effects [19]. On the other hand, T gate diminishes the gate resistance and enhances the cut-off frequency (f_T). But it also increases the electric field near the gate edges leading to early breakdown of the device [20]. To solve this issue, a double deck T-gate is used in the HEMT device. The double deck T-gate is formed using T-gate tied up with Si_3N_4 sheath as shown in Fig. 1. It provides an excellent mechanical reliability. In addition, it enhances the device breakdown voltage without sacrificing its maximum oscillation frequency (f_{MAX}) and cut off frequency (f_T). In this article, we demonstrate the impact of double deck T-gate on the DC and RF behaviour of L_G = 0.2 μm AlN/GaN HEMT using Silvaco Atlas TCAD tool. Furthermore, the merits and the drawbacks of added Silicon Nitride in the device is also summarized. This article is scheduled as follows. Section II provides the physics of a device structure and its dimension. Section III describes the physical model and calibration of a HEMT device. In section IV, the DC and RF performance of double deck T-gate HEMT is compared with

✉ D. Nirmal
dnirmalphd@gmail.com

1 Department of ECE, Karunya Institute of Technology and Sciences, Coimbatore, Tamil Nadu, India

2 Department of ECE, SR University, Warangal, Telangana, India

3 Department of ECE, Sri Ramakrishna Engineering College, Coimbatore, Tamil Nadu, India

4 Department of ECE, Anil Neerukonda Institute of Technology and Sciences, Vizag, Andra Pradesh, India

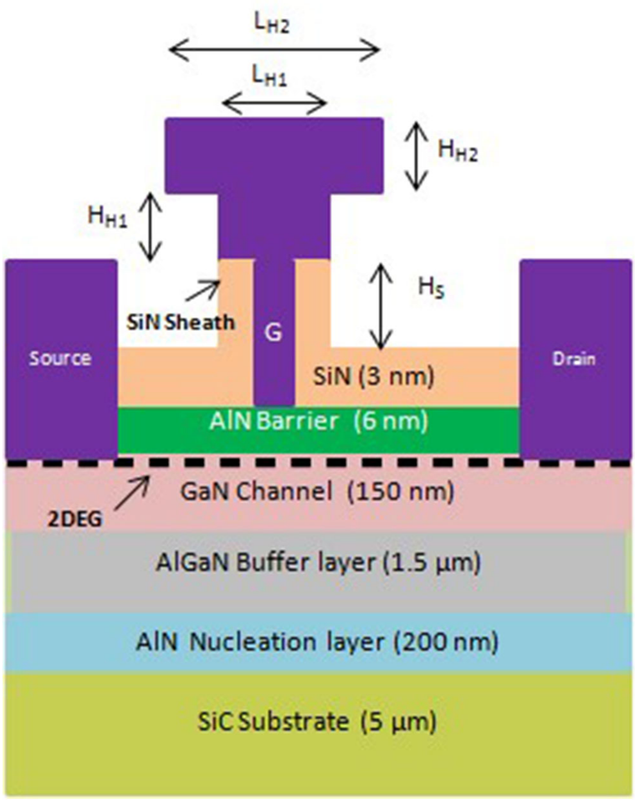

Fig. 1 Structure of L_G = 200 nm AlN/GaN/AlGaN HEMT devices a) Conventional HEMT b) T-gate based HEMT c) double deck T-gate based HEMT

the performance of conventional HEMT devices. Section V concludes this article.

2 SCHEMATICS OF L_G = 0.2 µm AlN/GaN HEMT DEVICES

The device structure of assorted AlN/GaN/AlGaN HEMTs are shown in Fig. 1. All the devices are simulated on 5 µm Silicon Carbide Substrate. The epitaxy comprises of a 200 nm Aluminium Nitride (AlN) nucleation layer, 1.5 µm Aluminium Gallium Nitride (AlGaN) buffer, 150 nm Gallium Nitride channel, 6 nm Aluminium Nitride barrier and 3 nm Silicon Nitride (Si_3N_4) passivation layer. The length of source and drain is defined as 0.5 um. The length (L_G) and width (W_G) of a gate is fixed to 200 nm and 200 µm respectively. The distance between the source and gate (L_{SG}) = 0.4 µm. The length between the gate and drain (L_{GD}) is fixed to 2 µm. The height of a stem (H_S) is defined as 200 nm. The height of first head (H_{H1}) and the height of second head (H_{H2}) are fixed as 50 nm. The length of first head (L_{H1}) and the length of second head (L_{H2}) are defined as 400 nm and 800 nm respectively. The Silicon Nitride (Si_3N_4) sheath supporting the T-gate enhances the mechanical reliability of a device. It also reduces the maximum electric field (E) near the gate edges to increase the off state breakdown voltage of a device. The double deck T-gate provides better gate control without sacrificing the operating frequency of a device. Owing to spontaneous and piezo-electric polarization, the two dimensional electron gas occurs at the junction of AlN barrier and GaN channel.

Hence, doping is not needed in this device [21]. The AlGaN buffer smoothes the lattice mismatch between the SiC substrate and Gallium Nitride channel. The material parameter used for TCAD simulation is described in Table 1.

3 Physical Models Used and Calibration of Simulator

The investigations of double deck T-gate on AlN/GaN/AlGaN HEMT is carried out using Silvaco Atlas TCAD simulator. To generate the electrons and holes, continuity equations, Poisson equations and drift diffusion models are included in the device simulation. Without any potential bias, the polarization charges are present at the interface of AlN/GaN layers. These charges are opposite in sign and equal in magnitude to sustain the device charge neutrality. The abstraction method to estimate the polarization charges was reported in [22]. A positive sheet charge density ($+\sigma_{pol}$) of 2×10^{13} cm^{-2} is fixed at the interface between the GaN and AlN region. The same concentration of equivalent negative sheet charge ($-\sigma_{pol}$) was defined at the interface of SiN/AlN layer. It is evident from [23] that the surface-donors are accountable for the creation of 2D-elctron gases in Gallium Nitride HEMT device. Therefore, donor-like surface traps with a density of 3.5×10^{13} cm^{-2} is defined at the interface of Si_3N_4/AlN having the energy of 0.2 eV over mid-gap band. The capture cross sections of hole (σ_p) and electron (σ_n) were presumed to be $\sigma_p = \sigma_n = 1 \times 10^{-15}$ cm^{-2}. To generate the charge carriers, constant-mobility and field-dependent mobility models are incorporated in the simulation. To include the electron generation and recombination, Shockley-Read-Hall model is used. In order to perform physical 2D simulation, it is necessary to carry out the

Table 1 Description of the material parameters [21]

Material Property	AlN	GaN
DOS-valence band (cm^{-3})	2.84×10^{20}	2.51×10^{19}
DOS-conduction band (cm^{-3})	4.1×10^{18}	2.24×10^{18}
Velocity saturation of an electron (cm/s)	1.5×10^{7}	9×10^{6}
Electron affinity (eV)	1.84	4
Relative permittivity	8.5	9.5
Bandgap energy (eV)	6.12	3.42
Electron mobility (cm^2/V s)	300	1000

calibration of physical simulator. In addition, the process of calibration is complicated and iterative. The important parameters for the device calibration are i) Velocity saturation of Gallium Nitride ii) mobility iii) surface charge iv) spontaneous polarization v) piezo-electric polarization vi) contact resistance of drain and source terminals vii) work function of gate, etc. The initial calibration is completed by fixing the work function of gate to 4.25 eV [21]. By adjusting the saturation velocity and low field mobility, the saturation and linear regions of drain current (I_D) are then calibrated. To enable the impact ionization effect in breakdown simulation, Selberherr model is used. In addition, Block Newton method with lattice heating models are incorporated to solve drift-diffusion equations [24]. The breakdown simulation shown in Fig. 12 have been calibrated with the experimental results reported in [25].

4 Results and Discussion

In this paper, the influence of T-gate and double deck T-gate on drain current (I_{DS}), transconductance (g_m), maximum oscillation frequency (f_{MAX}), Cut-off frequency (f_T) and breakdown voltage (BV) were analysed using Silvaco Atlas TCAD tool. The device model is simulated and calibrated for the W_G = 200 μm HEMT with gate length L_G = 200 nm, gate-source distance L_{GS} = 400 nm and the drain-gate distance L_{GD} = 2 μm.

The I_D-V_D curve of [21] is reproduced in this paper using Atlas TCAD simulation. It is obtained for the sweep of drain voltages (V_{DS}) between −1.4 V and + 1.4 V with a fixed gate bias of V_{GS} = 1 V. It is evident from Fig. 2 that the result of simulated I_D-V_D characteristics are in good agreement with the result reported in [21]. The conventional AlN/GaN HEMT exhibits the $I_{DS\text{-}max}$ of 380 mA/mm, where as AlN/GaN HEMT with T-gate and double deck T-gate exhibit a $I_{DS\text{-}max}$ of 440 mA/mm and 410 mA/mm respectively. T-gate based AlN/GaN/AlGaN HEMT shows 14% improvement in drain-source current (I_{DS}) compared to conventional HEMT device. It is because of small gate length and large gate area of T-shaped gate, reducing the overall gate access resistance [24]. In Gallium Nitride HEMT, gate to source/drain access region functions as curvilinear resistance which restricts the peak drain current.

The source/drain resistance comprises of bias free access region resistance ($R_{s/d}$) and contact resistance (R_c). The flow of current through the access region is expressed in eq. (1).

$$I_{acc} = Q_{acc}.v_s = Q_{acc}.\frac{v_{sat}.V_R}{\left[V_{R^\gamma sat} + V_{R^\gamma}\right]^{\frac{1}{\gamma}}} \tag{1}$$

Where γ is a fitting parameter, V_R is the potential drop across access region, V_{sat} is the saturation velocity of an electron, V_S is the velocity of electron and Qacc is the charge at access region. The source/drain resistance ($R_{s/d}$) can be given in terms of drain source current (I_{DS}) as expressed in eq. (2).

$$R_{s/d} = \frac{V_R}{I_{acc}} = \frac{R_{s_0/d_0}}{\left[1-\left(\frac{I_d}{I_{acc,sat}}\right)^{\gamma}\right]^{\frac{1}{\gamma}}} \tag{2}$$

It is clear from eq. (2) that ($R_{s/d}$) increases abruptly as drain current approaches to $I_{acc,sat}$ which restricts the flow of drain source current in the HEMT device. The I_{DS}-V_{GS} curve of L_G = 200 nm and W_G = 200 μm AlN/GaN/AlGaN HEMTs are depicted in Fig. 3. The Silicon Nitride (Si_3N_4) sheath under double deck T-gate includes additional access resistance ($R_{s/d}$) between the source and drain region. Hence, it reveals 7% reduction in drain current compared to the HEMT with T-shaped gate. The effectiveness of T-gate and double deck T-gate on the transconductance characteristics of W_G = 200 μm and L_G = 200 nm AlN/GaN/AlGaN HEMT devices are depicted in Fig. 4.

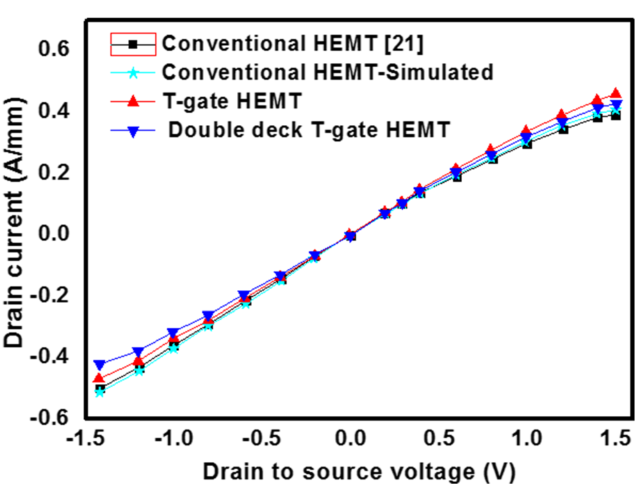

Fig. 2 I_{DS} Vs V_{DS} curve of L_G = 200 nm, W_G = 200 μm AlN/GaN/AlGaN HEMTs at V_{GS} = 1 V

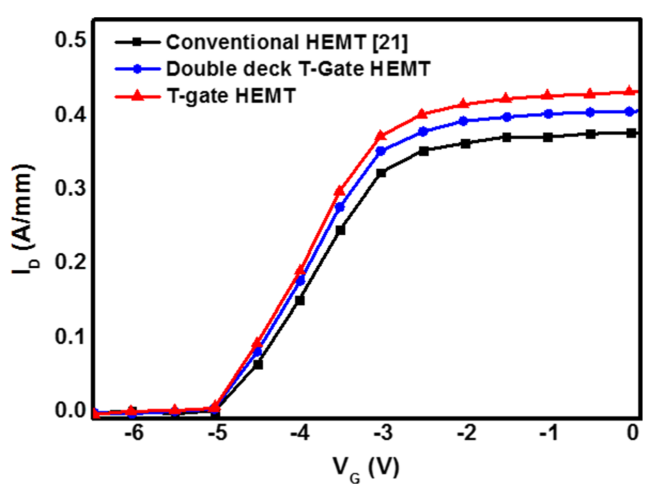

Fig. 3 I_{DS} Vs V_{GS} characteristics of L_G = 200 nm, WG = 200 μm AlN/GaN/AlGaN HEMTs

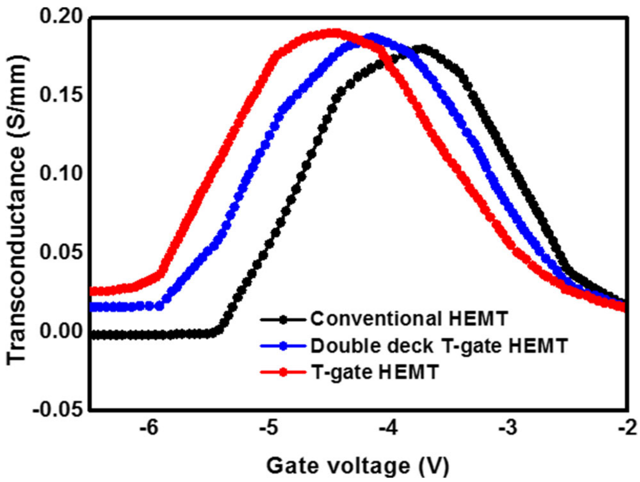

Fig. 4 Transconductance (g_m) Vs gate-source voltage curves of AlN/GaN/AlGaN HEMTs

The traditional HEMT achieves the maximum-transconductance ($g_{m\text{-}max}$) of 178 mS/mm, Where as the AlN/GaN HEMT with T shaped gate and double deck T-gate show the peak transconductance of 191 mS/mm and 186 mS/mm respectively. The general expression of $g_{m\text{-}max}$ is given in Eq. (3) [25].

$$g_{m-max} = \frac{\Delta_{I_D}}{\Delta V_{GS}} \tag{3}$$

Where, $g_{m\text{-}max}$ is the maximum transconductance in Siemens, ΔI_D is the variation in drain- current and ΔV_{GS} is the change in gate-source voltage. The extrinsic gate capacitance consists of two elements 1) fringing capacitances between the access region and gate stem and 2) parallel plate capacitances between the gate and neighbouring metals [26]. The variation of gate-source capacitance (C_{GS}) is obtained for the sweep of gate voltage (V_{GS}) between −7.5 V to 0 V at V_{DS} = 1 V as shown in Fig. 5. It is clear from Fig. 5 that the AlN/GaN/AlGaN HEMT with T-gate offers very low source to gate capacitance of 445 fF/mm. It is due to the high aspect ratios of T-gate stem to diminish the extrinsic capacitance [26]. If the height of T-gate stem is increased beyond 200 nm, there is no significant reduction in extrinsic capacitance is observed. It is because of the parasitic capacitance totally dominated by the capacitance owing to the stem alone. The traditional AlN/GaN HEMT reveals the source-gate capacitance of 5.9 × 10^{-13} F/mm, where as the HEMT with double deck T-gate exhibit the C_{GS} of 4.6 × 10^{-13} F/mm.

The double deck T gate uses SiN sheath to improve the gating efficiency, but it includes additional parasitic capacitance to the device affecting the overall AC performance of AlN/GaN/AlGaN HEMT. The change in gate-drain capacitance (C_{GD}) for the gate voltage sweep between −7.5 V to 0 V at V_{DS} = 1 V is illustrated in Fig. 6. It shows the maximum drain to gate-capacitance (C_{GD}) of 125 fF/mm for conventional HEMT device. Contrarily, the T-shaped gate HEMT and double deck T-gate HEMT offers the gate-drain capacitance (C_{GD}) of 108 fF/mm and 115 fF/mm respectively. In addition, the gate capacitance (C_G) = C_{GS} + C_{GD} exhibited for the conventional HEMT, T-gate HEMT and double deck T- gate HEMT are 692 fF/mm, 604 fF/mm and 668 fF/mm respectively as shown in Fig. 7.

The cut off frequency of Gallium Nitride HEMT is generally extracted as the sum of parasitic and intrinsic components given in Eq. (4) [20].

$$\tau = \frac{1}{2\pi f_T} = \frac{C_{GS}+C_{GD}}{g_m} + C_{GD}.(R_s+R_d)\left[1+\left(1+\frac{C_{GS}}{C_{GD}}\right)\frac{g_d}{g_m}\right] \tag{4}$$

$$f_{max} = \frac{f_T}{2\sqrt{(R_s+R_g).g_d + 2\pi f_T R_g C_{GD}}} \tag{5}$$

Where R_d, R_g, R_s, g_d, g_m, C_{GD}, C_{GS} denotes drain resistance, gate resistance, source resistance, drain conductance, transconductance, drain to gate capacitance and source to gate

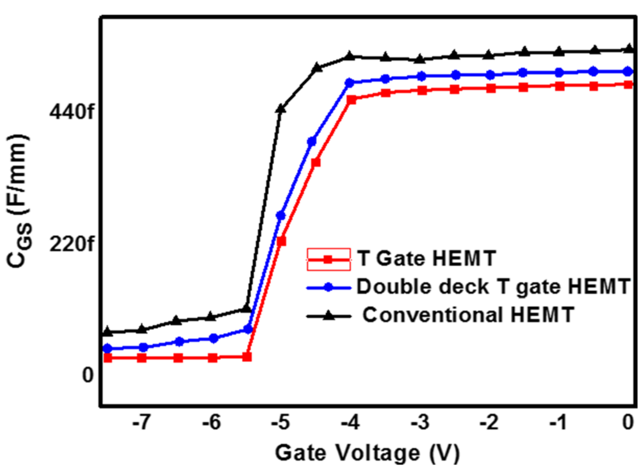

Fig. 5 Source to gate Capacitance (C_{GS}) Vs gate-source voltage (V_{GS}) curve of AlN/GaN/AlGaN HEMTs

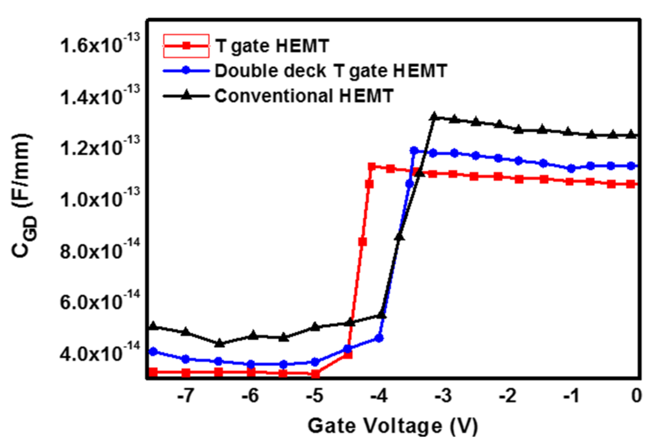

Fig. 6 Drain to gate Capacitance (C_{GD}) Vs gate to source voltage curves of AlN/GaN/AlGaN HEMTs

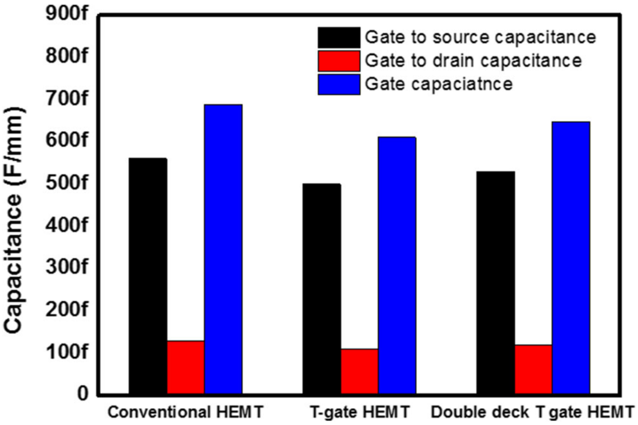

Fig. 7 Gate capacitance of Conventional HEMT, T-gate HEMT and double deck T-gate HEMT

capacitance respectively. The transient response of GaN HEMT is given by $\frac{C_{GS}+C_{GD}}{g_m}$, whereas the charging time is expressed as $C_{GD}.(R_s + R_d)$. Figure 8 shows the characteristics of unity current gain versus frequency of $L_G = 200$ nm AlN/GaN/AlGaN HEMT devices. The cut-off frequency (f_T) achieved for the HEMT with double deck T-gate lies between the cut-off frequencies of T-gate HEMT and conventional HEMT device. The current gain cut-off frequencies (f_T) achieved for the conventional HEMT, T-gate HEMT and double deck T-gate HEMT are 48.9 GHz, 66.2 GHz and 60 GHz respectively. The unilateral power gain versus frequency curve of $L_G = 200$ nm AlN/GaN/AlGaN HEMTs are depicted in Fig. 9. It offers the maximum-frequency $f_{MAX} = 99$ GH_Z for the conventional HEMT device. On the other hand, it produces the f_{MAX} of 118 GHz and 107 GHz for the AlN/GaN/AlGaN HEMT with T shaped gate and double deck T-gate respectively. The simulation results reveal higher f_{MAX} and f_T for T-gate HEMT compared to the conventional HEMT and double deck T-gate HEMT. It is due to small gate resistance and capacitance offered by T-gate HEMT. It is clear

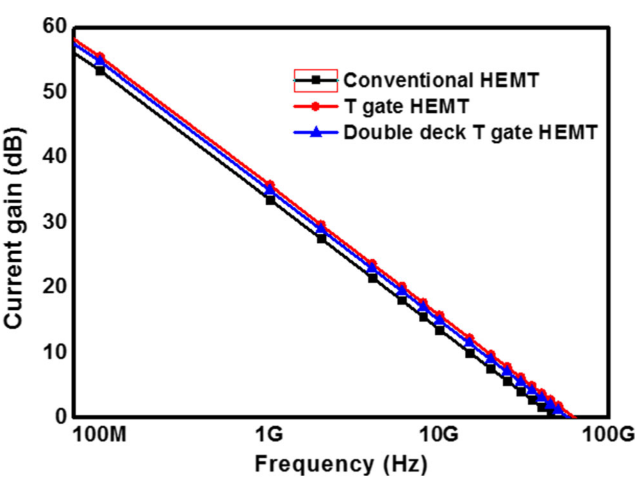

Fig. 8 Current gain Vs Frequency curve of Conventional HEMT, T-gate HEMT and double deck T-gate HEMT

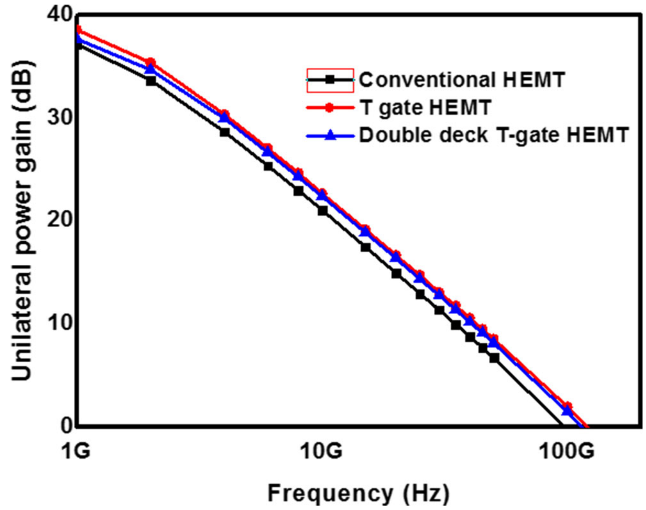

Fig. 9 Power gain Vs Frequency curve of Conventional HEMT, T-gate HEMT and double deck T-gate HEMT

from Fig. 9 that the f_{MAX} of double deck T-gate HEMT is less compared to the f_{MAX} of T-gate HEMT. It is mainly due to the inclusion of Si_3N_4 sheath under tri-layer T-gate head, which additionally contributes the parasitic capacitance to the device.

The electric field profiles of assorted AlN/GaN/AlGaN HEMTs are shown in Fig. 10. It exhibits the peak electric-field at drain-edge of gate terminal. It offers the electric-field E = 2.9 MV/cm for T-gate based HEMT, whereas the electric field achieved for conventional HEMT and double deck T-gate HEMT are 2.65 MV/cm and 2.1 MV/cm respectively. The simulation results confirm that the double deck T-gate HEMT exhibit very low electric field compared to conventional HEMT and T-gate HEMT. It is due to the incorporation of Si_3N_4 sheath and additional T-gate head in the device.

It reduces the crest electric-field at drain-edge of gate terminal that improves the device breakdown voltage and mechanical reliability. In Fig. 10, the electric field of the proposed device have additional peaks at about 1.2 um; it is due to the second head of T-gate on the top of the $S_{i3}N_4$ sheath acts like a field plate with a short distance to the semiconductor, effectively suppressing the peak field around the edges. The potential distribution of assorted AlN/GaN/AlGaN HEMTs are depicted in Fig. 11. As the drain to source voltage increases, the distribution of potential at drain edge is also increases.

It is because of the increased electric field between the drain and gate regions [27]. Figure 12 shows the off state breakdown behaviour of $L_G = 200$ nm and $W_G = 200$ µm AlN/GaN/AlGaN HEMT devices at $V_{GS} = -10$ V. The two major components of breakdown mechanism in HEMT devices are 1) Gate associated breakdown and 2) Bulk associated breakdown. Gate associated breakdown is mainly due to the gate-drain leakage current. It is because of the contamination or defects creating a path way for surface conduction [28–30].

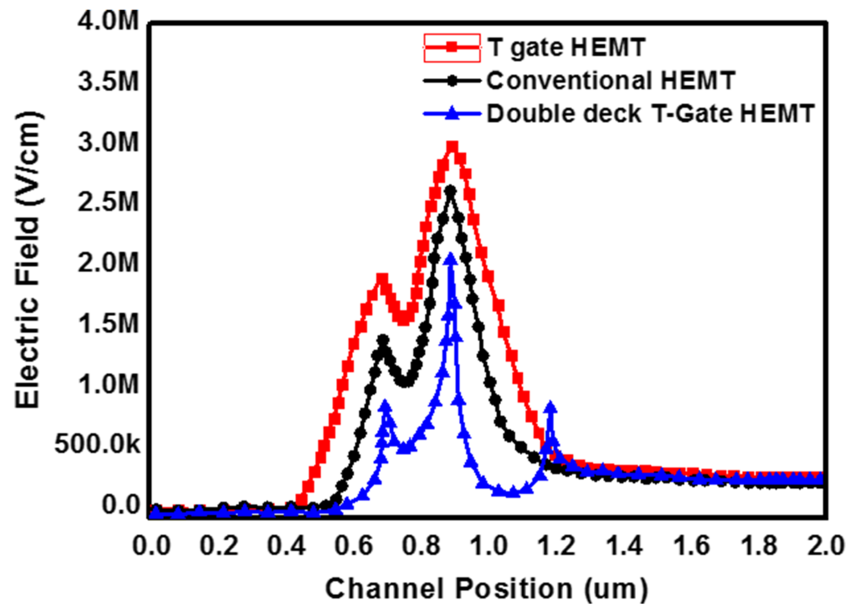

Fig. 10 Distribution of electric field in Conventional HEMT, T-gate HEMT and double deck T-gate HEMT

In order to reduce the gate-drain leakage, Si_3N_4 sheath is used under double deck T-gate head. It suppresses the crest electric-field at drain-edge of gate terminal, which enhances the device breakdown voltage. On the other hand, the bulk associated breakdown is due to the vertical leakage current between the drain and bulk region [28]. It can be reduced by choosing thick AlGaN buffer layer. Figure 13 shows the drain leakage characteristics of L_G = 200 nm AlN/GaN/AlGaN HEMT devices. It offers a very low drain-source leakage current of 9×10^{-10} A/mm for the HEMT with double deck T-gate. It is due to the sandwich of strong Si_3N_4 sheath and second T-gate head. At the same time, the conventional and T-gate based HEMT exhibits the drain-source leakage current of 8.5×10^{-9} A/mm and 9×10^{-8} A/mm respectively. Hence, a significant improvement in breakdown voltage is achieved for the proposed L_G = 200 nm AlN/GaN high electron mobility transistor. It exhibits the off-state breakdown voltage (BV_{OFF}) of 136 V, whereas the conventional HEMT and T-gate HEMT offers the breakdown voltage (BV_{OFF}) of 75.4 V and 54 V respectively. HEMT with double deck T-gate exhibits the lowest peak electric fields at the edges of Si_3N_4 sheath, gate foot, and gate head. This suppression of peak field helps to efficiently reduce the impact ionization rate which in turn needs to the reduction of leakage current and improvement of breakdown voltage.

In order to achieve, the optimal breakdown voltage and cut-off frequency in the proposed double deck T-gate HEMT, the stem height (H_S), second head height (H_{H2}) and second head length (L_{H2}) are varied. Varying the stem height from 0 to 200 nm causes the significant degradation in the device capacitance. Further any increase in stem height has no effect on device capacitance. Hence, the height of T-gate stem is fixed to 200 nm. On the other hand, to check the trade-off between

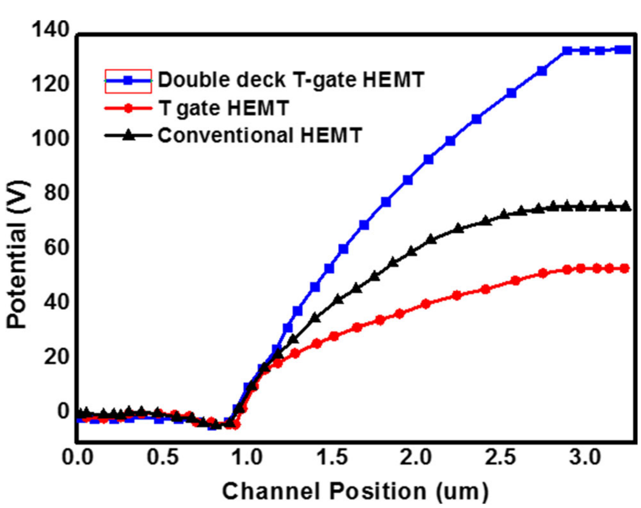

Fig. 11 Potential distribution of Conventional HEMT, T-gate HEMT and double deck T-gate HEMT

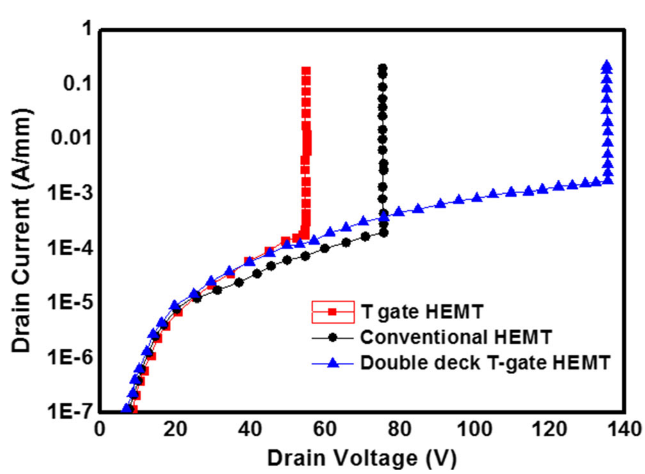

Fig. 12 Breakdown performance of Conventional HEMT, T-gate HEMT and double deck T-gate HEMT at V_{GS} = -10 V

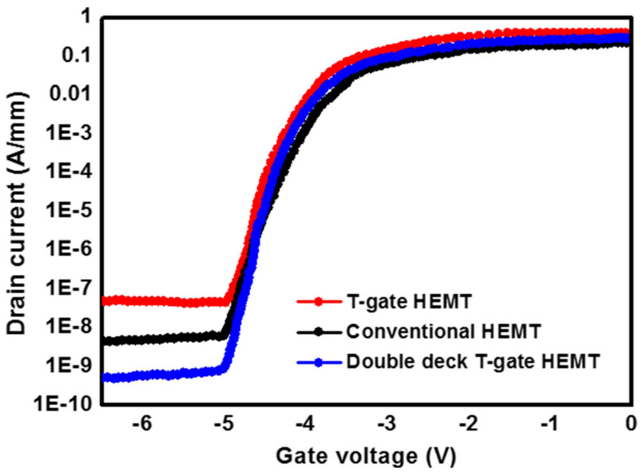

Fig. 13 Drain leakage current versus gate voltage curve of Conventional HEMT, T-gate HEMT and double deck T-gate HEMT

the cut-off frequency and breakdown voltage of the proposed device, the length (L_{H2}) and height (H_{H2}) of second head is varied as shown in Fig. 14 and Fig. 15 respectively. When the height of second head is increased from 10 nm to 90 nm, it reduces the gate access resistance gradually thereby increasing the transconductance and cut-off frequency of the proposed device. Contrarily, it reduces the device breakdown voltage as shown in Fig. 14, owing to the increased electric field near gate edges. As the length of second head increases from 400 nm to 1200 nm, it improves the smooth distribution of electric field over the device surface.

Hence, the breakdown voltage is enhanced from 110 V to 162 V as shown in Fig. 15. At the same time, it degrades the device cut-off frequency owing to its increased terminal capacitances (C_{GS} and C_{GD}). In both the plots (Fig. 14 and Fig. 15), the trade-off between the breakdown voltage and cut-off frequency is observed for different H_{H2} and L_{H2}. Therefore, Johnson figure of merit (breakdown voltage×cut-off frequency) is computed for the proposed device with various lengths and heights of the second head. It reveals the highest JFOM value of 7.9 Tera Hertz Volt at L_{H2} = 800 nm and H_{H2} = 50 nm.

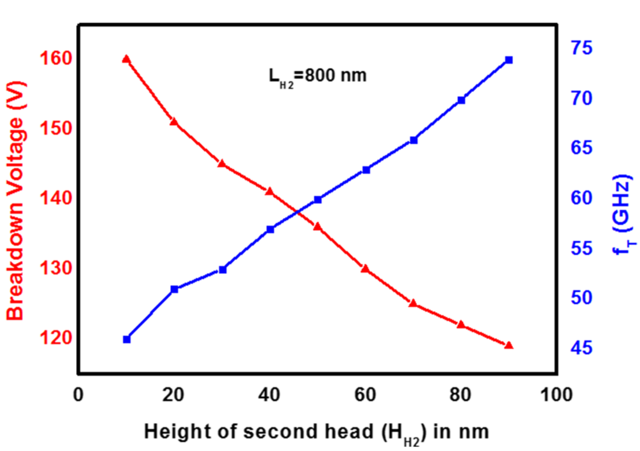

Fig. 14 Variation of breakdown voltage and cut-off frequency of double deck T-gate HEMT for different H_{H2} with fixed L_{H2}

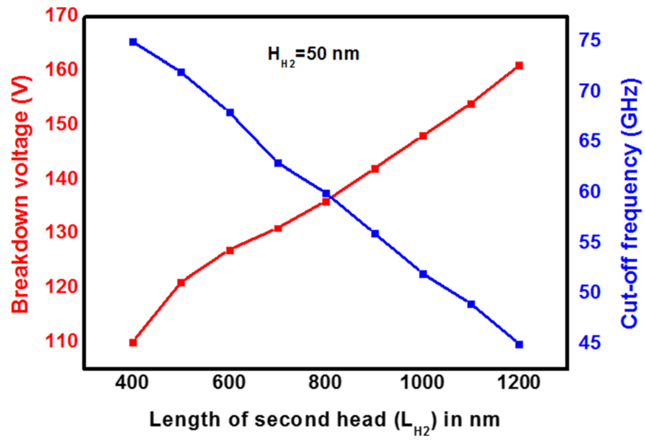

Fig. 15 Variation of breakdown voltage and cut-off frequency of double deck T-gate HEMT for different L_{H2} with fixed H_{H2}

5 Conclusion

The AlN/GaN/AlGaN HEMT combined with double deck T-gate and Si_3N_4 sheath provides an excellent AC and DC performance over conventional HEMT and T-gate based HEMT. It reveals 61% improvement in breakdown voltage over T-gate HEMT and 18% improvement in cut-off frequency over Conventional AlN/GaN HEMT. In addition, it exhibits a remarkable Johnson figure-of-merit ($f_T \times$ BV) of 7.9×10^{12} V/s for L_G = 200 nm and W_G = 200 μm AlN/GaN/AlGaN HEMT device. Furthermore, it has many advantages over T-gate HEMT and conventional HEMT. It exhibits high breakdown voltage, positive threshold voltage, enhanced gating efficiency and very good mechanical reliability. Hence, a double deck T-gate based AlN/GaN/AlGaN HEMT is an excellent device for 60 GHz V-band satellite application.

Acknowledgements The authors acknowledge the Centre for Research in Semiconductor Devices, Department of Electronics and Communication Engineering, Karunya Institute of Technology and Sciences, Coimbatore, India for providing all facilities to carry out this research work.

Authors' Contributions 1. A.S. Augustine Fletcher- TCAD Simulation and paper writing.
2. D. Nirmal- Idea and concept.
3. J. Ajayan-Idea and concept.
4. L. Arivazhagan- Idea and concept.
5. Husna Hamza- Paper editing and English correction.
6. P. Murugapandian-Paper editing and English correction.

Data Availability Not applicable.

Declarations

Ethics Approval and Consent to Participate "All procedures performed in studies were in accordance with the ethical standards of the institutional and/or national research committee and with the comparable ethical standards."

"For this type of study, formal consent is not required."

Consent for Publication Authors give consent for the publication of the Submitted Research article in Silicon.

Informed Consent "Not Applicable".

Conflict of Interest The authors declare that there is no conflict of interest reported in this paper.

Competing Interests The authors declare that they have no known competing financial interests.

Research Involving Human Participants and/or Animals "Not Applicable".

References

1. Augustine Fletcher AS, Nirmal D (2017) A survey of gallium nitride HEMT for RF and high power application. Superlat Micro Journ 109:519–537
2. Amano H, Baines Y, Beam E, Borga M, Bouchet T, Chalker PR, Charles (2018) The 2018 GaN power electronics roadmap. J Phys D Appl Phys 51:1–49
3. Herbecq N, Roch I, Linge A, Zegaoui M, Olivier P, Rouger N, Medjdoub F (2016) Above 2000V breakdown voltage at 600 K GaN-on- silicon high electron mobility transistors. Journ of Phys. Status Solid A 213(4):873–877
4. Augustine Fletcher AS, Nirmal D, Arivazhagan L, Ajayan J, Varghese A (2020) Enhancement of Johnson figure of merit in III-V HEMT combined with discrete field plate and AlGaN blocking layer. RF micro Comp-aid Eng 30(2):1–9
5. Wang Z, Cao J, Sun R, Wang F, Yao Y (2018) Numerical investigation on AlGaN/GaN short channel HEMT with AlGaN/InGaN/AlGaN quantum well plate. Superlat Microst 120:753–758
6. Singh SP, Chaturvedi N (2015) Influence of AlGaN and InGaN Back barriers on the performance of AlGaN/GaN HEMT. IETE Tech Rev 33(1):40–44
7. Keshmiri N, Wang D, Agrawal B, Hou R, Emadi A (2020) Current status and future trends of GaN HEMTs in electrified transportation. IEEE Acc 8:70553–70571
8. Nirmal D, Arivazhagan L, Augustine Fletcher AS, Ajayan J, Prajoon P (2018) Current collapse modeling in AlGaN/GaN HEMT using small signal equivalent circuit for high power application. Superlat Microst 113:110–120
9. Saito W, Suwa T, Uchihara T, Naka T, Kobayashi T (2015) Breakdown behaviour of high- voltage GaN-HEMTs. Microelec realiab:55(10): 1682–55(10): 1686
10. Li L, Nomoto K, Pan M, Li W, Hickman A, Miller J, Lee K, Hu Z (2020) GaN HEMTs on Si with regrown contacts and cutoff/maximum oscillation frequencies of 250/204 GHz. IEEE Elect Dev Lett 41(5):689–692
11. Denninghoff DJ, Dasgupta S, Lu J, Keller S, Mishra UK (2012) Design of High-Aspect-Ratio T-gates on N-polar GaN/AlGaN MIS-HEMTs for high f_{MAX}. IEEE Elect Dev Lett 33(6):785–787
12. Latorre-Rey AD, Albrecht JD, Saraniti M (2018) A ∏-shaped gate Design for Reducing hot-Electron Generation in GaN HEMTs. IEEE Trans Elect Dev 65(10):4263–4270
13. Wang Z, Chen W, Wang F, Cao J, Sun R, Ren K, Luo Y, Guo S, Wang Z, Jin X, Yang L, Zhang B (2018) Simulation study of AlGaN/GaN with Γ-shaped anode for ultra-low turn on voltage. Superlat Microst Jour 117:330–335
14. Maher H, Decobert J, Falcou A, Le Pallec M, Post G, Nissim YI, Scavennec A (1999) A triple channel HEMT on InP (camel HEMT) for large-signal high-speed applications. IEEE Trans Elect Dev 46(1):32–37
15. Hanawa H, Onodera H, Nakajima A, Horio K (2013) Similarities of lags, current collapse and breakdown characteristics between source and gate field-plate AlGaN/GaN HEMTs. IEEE Int Symp Realib Phys 24:152–156
16. Augustine Fletcher AS, Nirmal D, Ajayan J, Arivazhagan L (2019) Analysis of AlGaN/GaN HEMT using discrete field plate technique for high power and high frequency applications. Inter Jour Elect Comm 99:325–330
17. Bahat-Treidel E (2010) AlGaN/GaN/AlGaN DH-HEMTs breakdown voltage enhancement using multiple grating field plates (MGFPs). IEEE Trans Elect Dev 57(6):1208–1216
18. Hasan M, Tanvir MD, Asano T, Tokuda H, Kuzuhara M (2013) Current collapse suppression by gate field-plate in AlGaN/GaN HEMTs. IEEE Elect Dev Lett 34(11):1379–1381
19. Sehra K, Kumari V, Gupta M (2020) Optimization of π – gate AlGaN/AlN/GaN HEMTs for low noise and high gain applications. Silicon:1–8. https://doi.org/10.1007/s12633-020-00805-7
20. Murugapandiyan P, Ravimaran S, William J, Meenakshi Sundaram K (2017) Design and analysis of 30 nm T-gate InAlN/GaN HEMT with AlGaN back-barrier for high power microwave applications. Superlat Microst 111:1050–1057
21. Subramani NK, Sahoo AK, Nallatamby JC, Sommet R, Rolland N, Medjdoub F, Quére R (2016) Characterization of parasitic resistances of AlN/GaN/AlGaN HEMTs through TCAD-based device simulations and on-wafer measurements. IEEE Trans Micro Theo Tech 64(5):1351–1358
22. Ambacher O (1999) Two-dimensional electron gases induced by spontaneous and piezoelectric polarization charges in N- and Ga-face AlGaN/GaN heterostructures. J Appl Phys 85(6):3222–3233
23. Ibbetson JP, Fini PT, Ness KD, DenBaars SP, Speck JS, Mishra UK (2000) Polarization effects, surface states, and the source of electrons in AlGaN/GaN heterostructure field effect transistors. Appl Phys Lett 77(2):250–252
24. P Murugapandiyan, Md. Tanvir Hasan, V Rajya Lakshmi, Mohd Wasim, J Ajayan, N Ramkumar & D Nirmal (2020) Breakdown voltage enhancement of gate field plate $Al_{0.295}Ga_{0.705}N$/GaNHEMTs, International Journal of Electronics, DOI: 10.1080/00207217.2020.1849819, 1-18
25. Shreepad Karmalkar, Umesh K. Mishra,"Very high voltage AlGaN/GaN high electron mobility transistors using a field plate deposited on a stepped insulator", Sol-Stat Electron Dev,45 (9), 1645–1652 (2001)
26. Ghosh S, Ahsan SA, Chauhan YS, Khandelwal S (2016) Modeling of source/drain access resistances and their temperature dependence in GaN HEMTs. IEEE Inter Con Elect Dev Sol Stat Circts doi: https://doi.org/10.1109/EDSSC.2016.7785254
27. Saha G, Sen B, Deyasi A (2018) Calculating Transconductance of Nano-HEMT for different parasitic resistances and external biasing conditions. *Inter Con Elect, Mat Engg Nan-Tec*. https://doi.org/10.1109/IEMENTECH.2018.8465168
28. Bo S, Sensale-Rodriguez B, Wang R, Guo J, Hu Z, Yue Y, Faria F, Schuette M, Ketterson A, Beam E, Saunier P, Gao X, Guo S, Fay P, Jena D, Xing HG (2014) Effect of fringing capacitances on the RF performance of GaN HEMTs with T-gates. IEEE Trans Elect Dev 61(3):747–754

29. Kumar SP, Chaujar R, Gupta M, Gupta RS, Agrawal A (2007) Analytical modeling and simulation of potential and electric field distribution in dual material gate HEMT for suppressed Short Channel effects. *Asia-Pacific Microwav Conf* doi. https://doi.org/10.1109/APMC.2007.4554703
30. Meneghesso G, Meneghini M, Zanoni E (2014) Breakdown mechanisms in AlGaN/GaN HEMTs: an overview. Jap Jour App Phys 53(10):1–8